Photoisomerization Ability of Molecular Switches Adsorbed on Au(111): Comparison between Azobenzene and Stilbene Derivatives

Felix Leyssner,[†] Sebastian Hagen,[†] László Óvári,[†,||] Jadranka Dokić,[‡] Peter Saalfrank,[‡] Maike V. Peters,[§] Stefan Hecht,[§] Tillmann Klamroth,[‡] and Petra Tegeder*[,†]

Fachbereich Physik, Freie Universität Berlin, Arnimallee 14, D-14195 Berlin, Germany, Theoretische Chemie, Institut für Chemie, Universität Potsdam, Karl-Liebknecht-Str. 24-25, D-14476 Potsdam-Golm, Germany, and Department of Chemistry, Humboldt-Universität zu Berlin, Brook-Taylor-Str. 2, D-12489 Berlin, Germany

Received: October 9, 2009; Revised Manuscript Received: November 26, 2009

High resolution electron energy loss spectroscopy and two-photon photoemission was employed to derive the adsorption geometry, electronic structure, and the photoisomerization ability of the molecular switch tetra-*tert*-butyl-stilbene (TBS) on Au(111). The results are compared with the azobenzene analogue, tetra-*tert*-butyl-azobenzene (TBA), adsorbed on Au(111). TBS was found to adsorb on Au(111) in a planar (trans) configuration similar to TBA. The energetic positions of several TBS-induced electronic states were determined, and in comparison to TBA, the higher occupied molecular states (e.g., the highest occupied molecular orbital, HOMO) are located at similar energetic positions. While surface-bound TBA can be switched with light between its trans and cis configurations, in TBS this switching ability is lost. In TBA on Au(111), the trans → cis isomerization is driven by a substrate-mediated charge transfer process, whereby photogenerated hot holes in the Au d band lead to transient positive ion formation (transfer of the holes to the TBA HOMO level). Even though the energetic positions of the HOMOs in TBA and TBS are almost identical and thus a charge transfer should be feasible, this reaction pathway is obviously not efficient to induce the trans → cis isomerization in TBS on Au(111). Quantum chemical calculations of the potential energy surfaces for the free molecules support this conclusion. They show that cation formation facilitates the isomerization for TBA much more pronounced than for TBS due to the larger gradients at the Franck−Condon point and the much smaller barriers on the potential energy surface in the case of the TBA.

Introduction

Photochromes, commonly referred to as molecular switches, permit the control of molecular structure and resulting functional properties via excitation with light at appropriate wavelengths. Thereby the molecules are interconverted reversibly between at least two (meta) stable states as a result of a trans ⇌ cis isomerization, a photocyclization, or a combination of both. Among the most representative photochromes, stilbene, azobenzene, and their derivatives undergo a reversible photoinduced trans ⇌ cis isomerization (see Figure 1a) between the planar, thermodynamically more stable trans isomer and the three-dimensional cis form. Optical excitation followed by a rotation around the C═C (N═N) double bond in stilbene (azobenzene) or N inversion in azobenzenes drives the photoisomerization. In the case of azobenzene and its derivatives also a thermally activated cis → trans reaction is possible. In contrast, for stilbenoid compounds the thermal back reaction is unlikely since the activation barrier (E_a) is on the order of 1.9 eV[1−4] and thus much higher as compared to azobenzenes ($E_a \approx 1$ eV; see Figure 1b).[4−7]

Recently, increasing interest has been directed toward research on molecular switches at surfaces due to their potential use in nanotechnology ranging from information storage and processing to adaptive surfaces.[4,8−10] A major goal, relevant to the development of future applications, is to understand and control structural changes of molecular switches, such as azobenzenes and stilbenes adsorbed on solid substrate surfaces. For this purpose, it is crucial to gain a detailed knowledge about the adsorption geometry (molecular orientation) and the electronic structure, i.e., occupied and unoccupied electronic states (or band structure) of the molecules in contact with (metal) substrates.

In this contribution we examine the electronic and geometrical structure of 3,3′,5,5′-tetra-*tert*-butyl-stilbene (TBS, see Figure 1a) adsorbed on Au(111) using two-photon photoemission (2PPE) and high resolution electron energy loss spectroscopy (HREELS), respectively. This study is motivated by our previous work on 3,3′,5,5′-tetra-*tert*-butyl-azobenzene (TBA, see Figure 1a) on Au(111) with the intention of analyzing the adsorption, electronic, and in particular switching properties of the adsorbed molecules when changing the central functional unit from the diazo-group (−N═N−) in azobenzene to the vinylene-group (−HC═CH−) in stilbene. The four lateral *tert*-butyl groups in TBS and TBA increase the separation between the molecules and the substrate. This leads to a reduced electronic coupling between the active part of the molecule, i.e., the π -system, and the metal surface and thus allows for photoinduced and thermally activated isomerization in the case of TBA adsorbed on Au(111).[11−15] It has been demonstrated that the trans ⇌ cis isomerization of TBA on Au(111) is accompanied by reversible changes in the geometrical and electronic structure of the molecules enabling quantitative and mechanistic insights into the switching process.[16] On the other hand, light-induced

* To whom correspondence should be addressed. E-mail: petra.tegeder@physik.fu-berlin.de.
[†] Freie Universität Berlin.
[‡] Universität Potsdam.
[§] Humboldt-Universität zu Berlin.
[||] Current address: Reaction Kinetics Research Laboratory, Chemical Research Center of HAS, Szeged, Hungary.

10.1021/jp909684x
Published on Web 12/18/2009

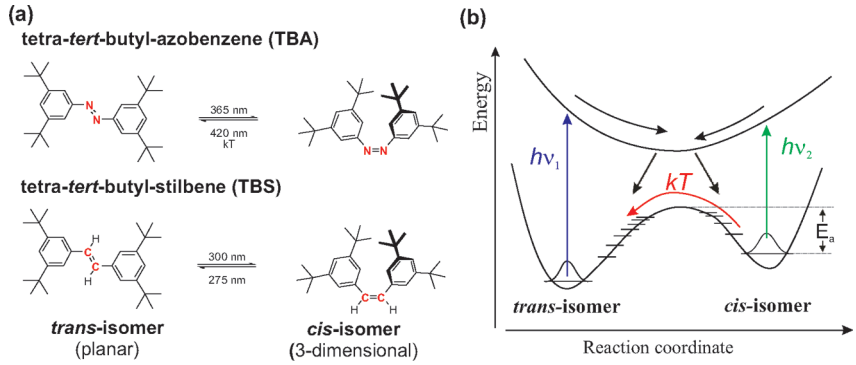

Figure 1. (a) Photochromic systems considered in this study. Azobenzene, stilbene, and their derivatives undergo a reversible photoinduced trans ⇌ cis isomerization. (b) Scheme of the reversible trans/cis isomerization induced by light at appropriate wavelengths and the thermal activated cis → trans reaction for molecular switches in the liquid or gas phase (for simplicity only one excited state is shown).

switching could not be achieved for TBA on Ag(111)[17] and the parent (unsubstituted) azobenzene on Au(111).[12] Presumably this arises from the stronger interaction with the metal substrate and corresponding differences in the geometric and electronic structure as well as the ultrashort lifetimes of the excited states.

Beside studies on the adsorption behavior of stilbenes adsorbed on Cu(110),[18] Si(100),[19] and Ag/Ge(111)-$\sqrt{3}$,[20,21] respectively, photoinduced trans ⇌ cis isomerization of the parent unsubstituted stilbene on Ag/Ge(111)-$\sqrt{3}$ has been observed by scanning tunneling microscopy (STM).[22] Thereby a biexciton-assisted photoisomerization model has been proposed in order to explain the optically induced conformational change of stilbene pairs. In contrast, no photoisomerization of stilbene adsorbed on Al_2O_3 (0001) has been observed.[23]

2PPE and HREELS is employed to study the electronic and geometrical structure as well as the isomerization ability of TBS on Au(111). It is found that TBS adopts a planar (trans) configuration in the low-coverage regime (≤1 ML) just as TBA does on Au(111). From the photoemission experiments TBS-derived unoccupied and occupied electronic states are obtained and their energetic positions are similar for TBA and TBS. However, in contrast to TBA no photoinduced changes in the electronic or vibrational structure are observed for TBS and thus, we propose a quenching of the photoisomerization in TBS/Au(111). The suppression of the light-induced conformational change is discussed on the basis of the photoisomerization mechanism operative in TBA on Au(111), namely the creation of a positive ion resonance. Apparently, this pathway is not efficient in TBS/Au(111), which is supported by quantum chemical calculations.

Methods

Synthesis and Isomerization in Solution. TBS was synthesized from the 3,5-di-*tert*-butylbromo-benzene via a four-step sequence involving Sonogashira coupling with TMSA followed by desilylation then hydroboration and finally Suzuki coupling with 3,5 di-*tert*-butylbromo-benzene. TBS was successfully characterized and the trans geometry verified by ^{1}H NMR. In cyclohexane solution, TBS displays the photochemical isomerization behavior typical for stilbene derivatives, which has been verified by UV/vis absorption spectroscopy (see the Supporting Information).

Both the HREELS and the 2PPE experiment were carried out under ultrahigh vacuum conditions. The Au(111) crystal was mounted on a liquid-nitrogen-cooled cryostat, which in conjunction with resistive heating enables temperature control from 90 to 750 K. The crystal was cleaned by a standard procedure of Ar^+ sputtering and annealing. The TBS was dosed by means of a home-built effusion cell held at 380 K at a crystal temperature of 260 K. The TBS coverage was quantified by thermal desorption spectroscopy (TDS) and work function measurements. In the TDS experiments, the substrate was resistively heated with a heating rate of 1 K/s and desorbing TBS was detected with a quadrupole mass spectrometer at the TBS-fragment mass of 190 amu (3,5-di-*tert*-butyl-phenyl ion).

High-Resolution Electron Energy Loss Spectroscopy. HREEL spectra were recorded in both specular ($\theta_i = \theta_r = 60°$) and off-specular ($\theta_i = 50.8°$, corresponding to 9.2° off-specular; $\theta_r = 60°$) scattering geometry. The energy of the primary electrons was set to 3.7 eV with an overall resolution of ≤3.5 meV, measured as the full width at half-maximum (fwhm) of the elastic peak. In the specular spectra of HREELS, the signals contain both dipole and impact scattering components.[24] The selection rule for dipole scattering at metal surfaces, i.e., only vibrations with a component of the dipole moment change normal to the surface are observable, is the same as that for infrared reflection absorption spectroscopy.[25] Therefore it is useful for characterizing the geometrical structure and predominantly the orientation of adsorbates. To separate the dipole-scattering components, off-specular spectra consisting only of impact-scattering components were measured.

Two-Photon Photoemission Spectroscopy. For the 2PPE measurements, femtosecond laser pulses are generated by a 300 kHz Ti:sapphire laser system, which pumps an optical parametric amplifier. The visible output with photon energies from 1.7 to 2.7 eV, respectively, is frequency doubled in a BBO crystal to generate ultraviolet pulses (3.4−5.4 eV photon energy). The laser pulses are incident on the surface with an angle of 45° with respect to the surface normal. While the pump pulse $h\nu_1$ excites an electron from below the Fermi level (E_F) to intermediate unoccupied states at energies $E - E_F = E_{kin} + \Phi - h\nu_2$ (with Φ the work function), the probe pulse $h\nu_2$ photoionizes the sample by lifting the excited electron above the vacuum level (E_{vac}). Photoelectrons are detected in an electron time-of-flight (TOF) spectrometer and are analyzed with respect to their kinetic energy (E_{kin}). The energy resolution of the TOF spectrometer depends on the electron energy, it is ∼10 meV at $E_{kin} \approx 1$ eV. Variation of the electron detection angle α with respect to the surface normal allows one to determine the electron momentum parallel to the surface $\hbar k_{\|}$ according to

$$\hbar k_{\|} = \sqrt{2m_e E_{kin}} \sin \alpha \qquad (1)$$

where m_e denotes the free electron mass. $k_{\|} = 0$ corresponds to electrons detected along the surface normal (α = 0). For

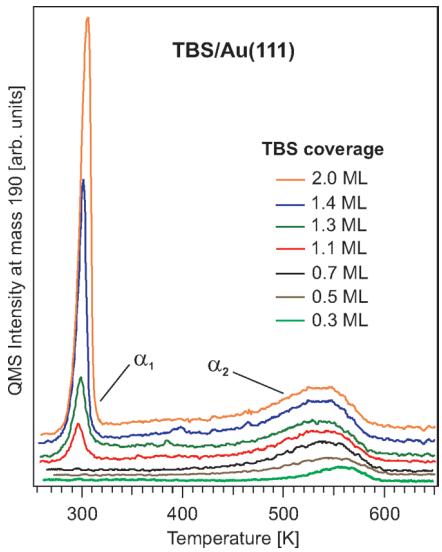

Figure 2. Thermal desorption spectra of TBS on Au(111) at different coverages recorded with a heating rate of 1 K/s at the fragment-mass of 190 amu (3,5-di-*tert*-butyl-phenyl ion).

dispersion measurements, the vacuum levels of the sample and spectrometer have to be balanced due to their different work functions by applying an appropriate bias voltage to the sample. Thereby, deformation of the angular distribution of the emitted electrons by electric fields is minimized.

Calculations. All quantum chemical calculations were done with the Gaussian 03[26] program package. The B3LYP[27] functional and a 6-31G* basis set[28−30] were used.

Results and Discussion

Adsorption Behavior of TBS on Au(111). In order to obtain insights into the adsorption properties of TBS/Au(111) and to quantify the coverage, thermal desorption spectra were recorded as a function of TBS coverage (Figure 2). At low coverage a broad desorption peak (α_2) is observed around 555 K, which extends to lower temperatures with increasing coverage. After saturation of this peak, a second desorption feature α_1 develops at 296 K. The α_1 peak increases in height and width with increasing coverage, showing a typical zero-order desorption behavior. We therefore assign this peak to desorption from the multilayer while the α_2 peaks is associated with desorption from the first monolayer (ML). The thermal desorption behavior of TBS from Au(111) is very similar to those of other aromatic compounds on noble metal surfaces, for example azobenzene derivatives,[11,17,31] benzene,[32,33] hexafluorobenzene,[34] and pyridine,[35] respectively. A common observation in these systems is the substantial broadening of the desorption peak with increasing coverage in the monolayer regime. This can be attributed to repulsive interactions between the adsorbed molecules (for example due to dipole−dipole interactions).

Figure 3a shows the HREEL spectrum of 1 ML TBS adsorbed on Au(111), which was prepared by heating the multilayer-covered surface to 400 K, recorded in specular scattering geometry. For comparison, the infrared (IR) spectrum obtained for the solid state (in KBr) is displayed in Figure 3b. The vibrational frequencies and their assignments for both the adsorbed and condensed TBS are listed in Table 1 together with the literature values of vibrational modes of 0.9 ML TBA adsorbed on Au(111)[13] and condensed *trans*-stilbene.[36−38]

The HREEL spectrum for the adsorbed TBS agree well with the IR data for TBS in the solid, only small shifts toward lower

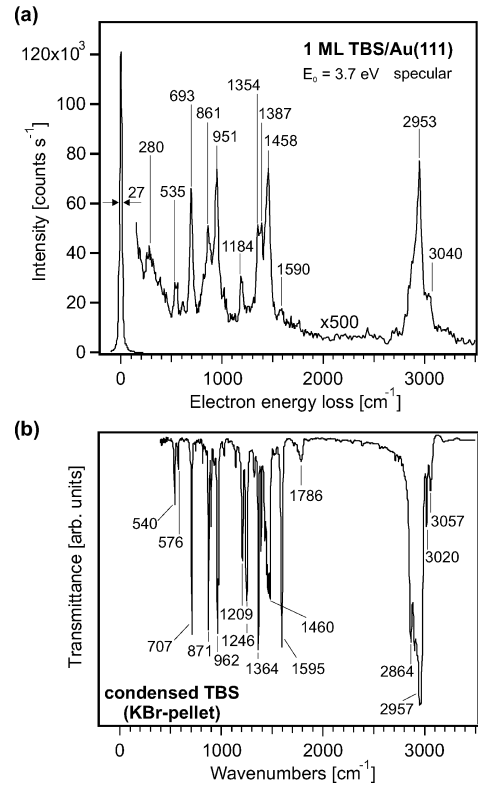

Figure 3. (a) HREEL spectrum of 1 ML TBS adsorbed on Au(111) recorded in specular scattering geometry with primary electron energy of 3.7 eV. The fwhm of the elastic peak is 27 cm^{-1} (3.3 meV). (b) Fourier-transform infrared spectrum of condensed TBS (KBr-pellet) measured with a resolution of 4 cm^{-1}.

energies are observed for some vibrations due to adsorption on Au(111). In both the adsorbed and condensed TBS the asymmetric CH_3 stretch mode ($\upsilon_{as} \approx 2953$ cm^{-1}) and the CH_3 deformation modes ($\delta_{as} \approx 1458$ cm^{-1}, δ_s around 1387 cm^{-1}) of the *tert*-butyl-groups as well as the out-of-plane C−H deformation of the phenyl rings and the ethylene moiety (γ(C−H) ≈ 861 cm^{-1}, γ (C−H)$_e$ ≈ 951 cm^{-1}) and the phenyl ring torsion mode (τ(C−C) ≈ 693 cm^{-1}) show high intensities. In contrast, the stretch modes of the aromatic rings (ν(C−C)) at 1246 and 1595 cm^{-1}, respectively, result in very high intensities in the IR spectrum of the condensed TBS, are absent or barely visible in the HREELS.

In order to gain insights into the excitation mechanism, i.e., dipole- versus impact-scattering, and to analyze the adsorption geometry of TBS on Au(111), we performed angular dependent measurements. Figure 4 shows a comparison of HREEL spectra recorded in specular and 9.2° off-specular geometries for 1 ML TBS/Au(111).

Most striking is the huge intensity decrease of the out-of-plane torsion mode of the phenyl rings (τ(C−C)) at 693 cm^{-1} and the C−H bending mode (γ(C−H)) at 861 cm^{-1} in the off-specular spectrum, indicating that their intensities are originating mostly from dipole scattering in the specular spectrum (see Table 1 for the assignment of the dipole active modes). The strong dipole activity of the phenyl ring torsion and C−H bending modes point toward a preferential orientation of the TBS parallel to the Au(111) surface, viz. a planar trans configuration, since in this orientation these modes have a strong dipole moment change upon vibration perpendicular to the surface. Moreover, the in-plane modes of TBS, for instance the stretch vibration of the phenyl rings at 1246 and 1595 cm^{-1} of condensed TBS observed with high intensities, are absent or barely visible in

TABLE 1: Vibrational Frequencies (in cm^{-1}) and Assignments for 1 ML TBS Adsorbed on Au(111) and Condensed TBS, Respectively

vibrational mode[a]	1 ML TBS[b]	cond. TBS[c]	0.9 ML TBA[d]	*trans*-stilbene[e]
δ(C−X), τ(C−X)	187			198
τ(C−C)^{Ar}	254		275	268
τ(C−C)^{Ar}	280		299	291
δ(C−X), τ(C−C)^{Ar}	319			336
τ(C−C)^{Ar}, δ(C−X)	429			410, 419
τ(C−C)^{Ar}	451			455
γ(C−X)	535 (da)[f]	540		528
δ(C−C)^{Ar}	558	576	543	541
δ(C−C)^{Ar}	609	630		620
τ(C−C)^{Ar}	693 (da)	707	696	692
γ(C−H)^{Ar}, ν(C−C)^{Ar}	816	813		847, 824
γ(C−H)^{Ar}	861 (da)	871, 889	879	848
γ(C−H)$_e$	951	962		966
ν(C−C)^{Ar}, δ(C−H)^{Ar}	1019	1026	1008	1028
ν(C−C)^{Ar}, δ(C−H)^{Ar}	1038	1026		1059
δ(C−H)^{Ar}	1184	1209	1189	1187
ν(C−C)^{Ar}		1246		1234
$\delta_s(CH_3)^t$	1354	1364	1359	
$\delta_s(CH_3)^t$	1387	1390	1385	
$\delta_s(CH_3)^t$	1458	1460, 1477	1453	
ν(C−C)^{Ar}	1590	1595	1584	1597
$\upsilon_s(CH_3)^t$	2847, 2876	2864	2878	
$\upsilon_{as}(CH_3)^t$	2953	2957	2963	
ν(C−H)$_e$	3011	3020		3029
ν(C−H)^{Ar}	3040	3057	3057	3040

[a] CX stands for the phenyl ring-ethylene bond; e, indicates the ethylene moiety; s, symmetric; as, asymmetric; υ, stretch; δ, in-plane bend; τ, torsion; γ, out-of-plane bend; Ar, aromatic ring; t, *tert*-butyl group. [b] Obtained by HREELS; present study. [c] IR spectrum recorded in KBr; present study. [d] HREELS data from tetra-*tert*-butyl-azobenzene (TBA) adsorbed on Au(111) adapted from ref 13. [e] IR and Raman data adapted from refs 36−38. [f] The da indicates a strong dipole activity.

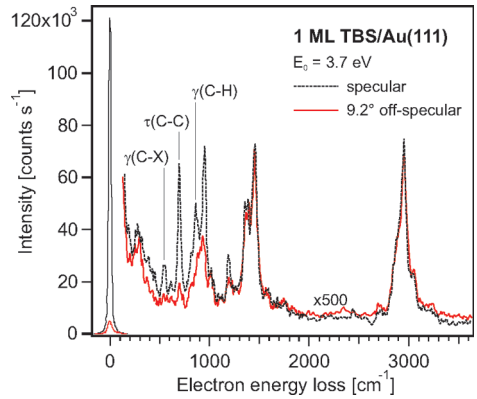

Figure 4. HREEL spectra of 1 ML TBS adsorbed on Au(111) recorded in specular and 9.2° off-specular scattering geometry, respectively, with a primary electron energy of 3.7 eV.

the HREELS of the adsorbed species. This corroborates the proposed planar adsorption geometry. In addition, STM measurements show that in the low-coverage regime TBS forms well-ordered islands with the molecules adsorbed in the planar configuration.[39] Hence, we conclude that the adsorption behavior is similar to the one observed for TBA in direct contact with the Au(111) surface.[13,40,41] Note that also in the liquid phase the trans isomer of both azobenzene and stilbene is known to be the energetically favorable configuration.[2]

Electronic Structure of TBS on Au(111). In order to gain knowledge about the electronic structure, i.e., occupied and unoccupied electronic states of surface-bound TBS, we performed 2PPE. Figure 5a shows two-color 2PPE spectra of the clean Au(111) surface and of 1 ML TBS adsorbed on Au(111)

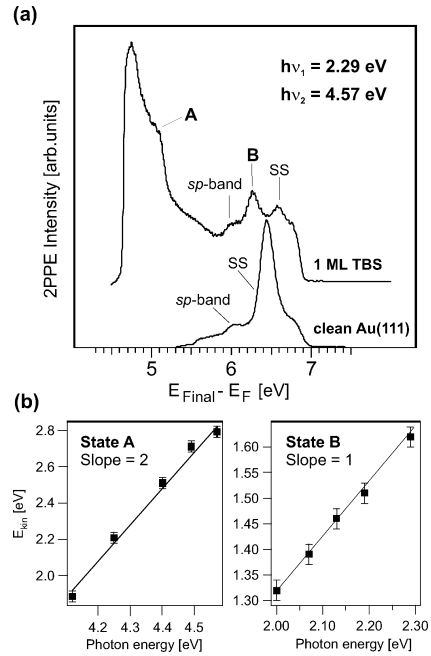

Figure 5. (a) Two-color 2PPE spectra from the bare Au(111) surface and 1 ML TBS adsorbed on Au(111) measured with 2.29 and 4.57 eV photons. The spectra are displayed as a function of final state energy above the Fermi level, $E_{Final} - E_{Fermi} = E_{kin} + \Phi$. (b) Photon energy dependence of the peaks labeled as A and B in the 2PPE spectrum of TBS/Au(111). The symbols are experimental data, and the solid lines are fits. The kinetic energy of peak A varies with $2\Delta h\nu$, while the kinetic energy of peak B varies with $1\Delta h\nu$. This indicates that peak A originates from an occupied initial state, whereas peak B evokes from an unoccupied intermediate state in the 2PPE process.

recorded at photon energies of 2.29 and 4.57 eV. From the clean Au(111) an intense peak at $E_{Final} - E_F = 6.4$ eV is observed, which can be assigned to the occupied Shockley surface state (SS). The energetic position is −0.46 eV with respect to E_F in accordance with previous work.[42] The peak at 6 eV results from the sp band of Au(111) located at −0.86 eV below the Fermi level.[43,44] Deposition of 1 ML TBS leads to the appearance of two new features around 5 eV (peak A) and 6.25 eV (peak B) in the 2PPE, whereas the surface state loses intensity and shifts by ∼100 meV from −0.46 to −0.34 eV with respect to E_F. In order to identify whether the peaks A and B originate from occupied initial states, unoccupied intermediate states, or unoccupied final states in the 2PPE process, their dependence on photon energy was investigated. If an electron is excited directly from an occupied state below the Fermi level in a 2PPE process by adsorption of two photons, the shift in the electron kinetic energy ΔE_{kin} scales with 2 $\Delta h\nu$ ($\Delta h\nu = h\nu_1 - h\nu_2$). If 2PPE involves one-photon excitation of an electron into an unoccupied intermediate state (between E_F and E_{vac}) followed by photoionization of this transient state, ΔE_{kin} scales with 1 $\Delta h\nu$. In the case of an unoccupied final state E_{kin} is constant.

Figure 5b shows the photon energy dependence of the peaks A and B. The kinetic energy of peak A varies with $2\Delta h\nu$, indicating that the peak is caused by photoemission from an occupied initial state. This occupied state is located 1.75 eV below E_F. In contrast, the peak labeled as B scales with $1\Delta h\nu$ suggesting that peak B arises from an unoccupied intermediate state. This state is pumped with the UV pulse $h\nu_2$ and probed with the visible pulse $h\nu_1$, therefore its energetic position is 3.9 eV above E_F or 0.75 eV below E_{vac} (Φ(1 ML) = 4.65 eV).

Figure 6 displays a one-color 2PPE spectrum of 1 ML TBS adsorbed on Au(111) recorded at a photon energy of 4.57 eV.

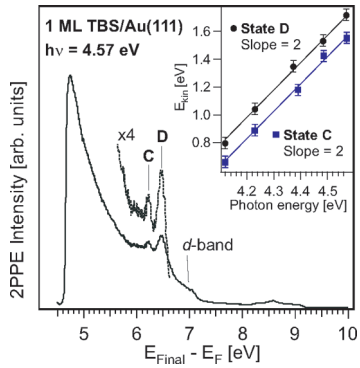

Figure 6. One-color 2PPE spectrum from 1 ML TBS adsorbed on Au(111) recorded at a photon energy of 4.57 eV. The inset shows the photon energy dependence of the peaks labeled as C and D in the 2PPE spectrum of TBS/Au(111). The symbols are experimental data, and the solid line is a fit. The kinetic energy of both peaks vary with $2\Delta h\nu$, indicating that they originate from occupied electronic states.

TABLE 2: Calculated Molecular Orbital Energies (in eV) with Respect to Energy of the HOMO of TBS

molecular orbitals	TBS
LUMO+2	5.54
LUMO+1	5.52
LUMO	4.07
HOMO	0.00
HOMO-1	–1.10
HOMO-2	–1.11
HOMO-3	–1.43

Besides photoemission from the occupied d band,[43,44] which is located at ~2.0 eV below E_F, the features labeled as C and D are observed. The inset of Figure 6 shows the photon energy dependence of these peaks. The kinetic energy of both photoemission peaks vary with $2\Delta h\nu$, indicating that the transitions involve occupied initial states. Thus the energetic positions of the states C and D are −2.9 and −2.65 eV below E_F, respectively.

Assignment of the Electronic States. In order to assign the TBS-derived occupied and unoccupied states to photoemission from specific molecular orbitals (MOs), we calculated the orbital energies for geometry-optimized gas phase TBS on the B3LYP/6-31G* level of theory. The analysis of state-transitions in the molecular orbital (one electron) picture is only approximate, and also the idealization of the physisorbed species as a free molecule introduces errors. With these warnings in mind, we show in Table 2 the calculated orbital energies with respect to the highest occupied molecular orbital (HOMO) of TBS. All molecular orbitals considered in this study have π symmetry. While the HOMO has a bonding character at the central C═C bond, the LUMO possesses a nodal plane (antibonding character) through the C═C bond. The HOMO-1 and HOMO-2 are localized at the phenyl rings with no charge density at the C═C bridge. Both orbitals are nearly degenerate. The HOMO-3 is also located at the phenyl rings but with some charge density at the C═C bridge. The LUMO+1 and LUMO+2 are concentrated mainly at the phenyl rings. These orbitals possess positive absolute energies, i.e., they are located above the vacuum level (final states). Note that for larger basis sets, an increasing number of diffuse "Rydberg-like" MOs emerge in the energy regime close to the vacuum level.

Returning to the assignment of the 2PPE signals of TBS/Au(111), the occupied initial state labeled as A, which exhibits an energetic position of −1.75 eV with respect to E_F, arises predominantly from ionization of the HOMO. On the basis of

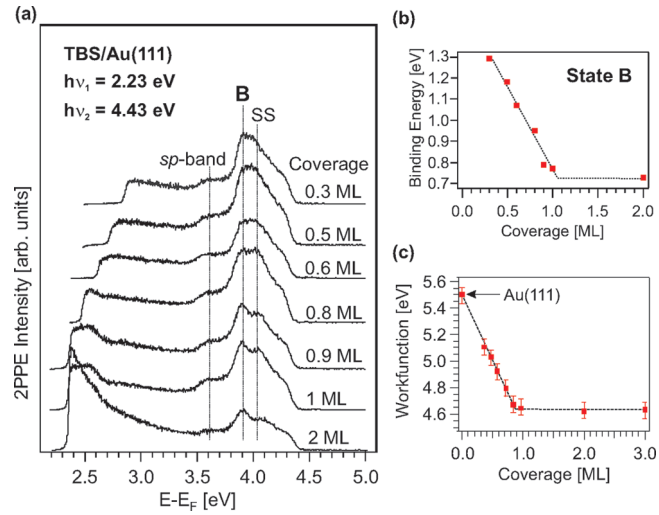

Figure 7. (a) Two-color 2PPE spectra recorded at photon energies of 2.23 and 4.43 eV of various TBS coverages. The spectra are displayed as a function of intermediate state energy above E_F, $E - E_F = E_{kin} + \Phi - h\nu_{probe}$, where $h\nu_{probe}$ is the probing photon energy. (b) Binding energy (with respect to E_{vac}) of the unoccupied intermediate state (peak labeled as B) as a function of TBS coverage. (c) Work function (Φ) of TBS/Au(111) as a function of coverage. Φ is determined by the low energy cutoff (vacuum level, E_{vac}) and high energy cutoff (Fermi edge, $E_{FE} = E_F + 2h\nu$) of the photoemission spectra, by the relation $\Phi = 2h\nu - (E_{FE} - E_{vac})$, where $h\nu$ is the photon energy used in the one-color 2PPE experiment.

the calculated orbital energies we attribute the peak labeled as D at −2.65 eV to photoemission from the HOMO-1 and HOMO-2, since these orbitals are nearly degenerate. Accordingly, the 2PPE signal at −2.9 eV (peak labeled as C) results from ionization of the HOMO-3. The unoccupied intermediate state (peak B) exhibits an energetic position of 3.9 eV above E_F, thus a binding energy of 0.75 eV with respect to E_{vac} at a coverage of 1 ML. Since the first image potential state ($n = 1$) of the clean Au(111) surface is also located in this energy region, possessing a binding energy of 0.8 eV,[45] we carried out coverage and angular dependent 2PPE measurements in order to understand the nature of this electronic state.

Figure 7a displays a set of two-color 2PPE spectra taken at photon energies of 2.23 and 4.43 eV at various TBS coverages. As can be seen from Figure 7a, the energetic position of the unoccupied state (peak B) does not change as a function of coverage: it stays constant at 3.9 eV. Accordingly, its binding energy with respect to E_{vac} changes; that is, it increases from 0.75 to 1.3 eV with decreasing coverage from 2 to 0.3 ML (see Figure 7b) and follows the shift in the work function as a function of TBS coverage, as shown in Figure 7c, viz. the binding energy increases with increasing work function. Thus, this state is not pinned to the vacuum level, as normally expected for image potential states. To gain insight into the extent of electron delocalization parallel to the surface we performed dispersion measurements using angle-resolved 2PPE. Figure 8 shows the dependence of the kinetic energy on $k_{||}$ for 1 ML TBS adsorbed on Au(111) measured at a photon energies of 4.59 and 2.31 eV. The dispersion curves can be described by a parabolic function $E_{kin}(k_{||}) = \hbar^2 k_{||}^2/2m_{eff} + E_{kin}(k_{||} = 0)$, where m_{eff} is the effective electron mass. The fits give an effective electron mass of $3.4 \pm 0.1 m_e$ for 1 ML and $3.2 \pm 0.2 m_e$ for 2 ML (data not shown), which indicates that the electronic potential is strongly modulated parallel to the surface and the wave function of state B is not free-electron like. This relatively high effective electron mass could be explained by the assump-

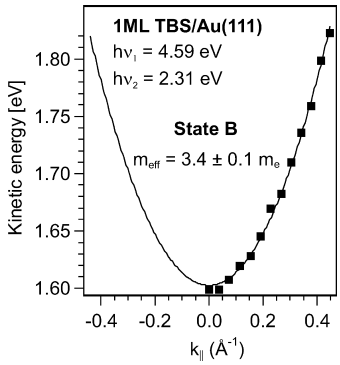

Figure 8. Dispersion of the peak B for 1 ML TBS adsorbed on Au(111) recorded at photon energies of 4.59 and 2.31 eV.

tion that state B originates from a molecular orbital of TBS, i.e., from a state with a localized character. The constant energetic position at 3.9 eV above E_F of this state as a function of coverage corroborates this assumption; therefore, we assign this peak B to an unoccupied molecular orbital of TBS. Whether this peak arises from the lowest unoccupied molecular orbital (LUMO) or a higher lying unoccupied molecular state (LUMO+n) will be discussed in the following.

The optical gap ($\pi \rightarrow \pi^*$ excitation) determined by UV−vis spectroscopy of *trans*-TBS in cyclohexane is ∼4.1 eV (λ_{max} = 300 nm). Using time-dependent density functional theory (TD-B3LYP/6-31G*) for the *trans*-TBS optimized in the gas phase, we find a lowest excitation energy of 3.86 eV (321 nm). The signal is dominated by the HOMO (π) → LUMO (π^*) transition. The computed HOMO−LUMO energy difference is 4.07 eV, showing that the one-electron picture describes this excitation well. Taking the energy difference between the measured peaks labeled as A and B, on the other hand, gives a gap of 5.65 eV, which is far too large to be compatible with the HOMO → LUMO transition. Depending on the electronic coupling strength between the molecules and the metallic substrate one would expect a even smaller gap compared to the free molecule. In addition, the unoccupied electronic state is most likely transiently populated *via* an electron transfer from the metal to the molecule. This negative ion resonance is stabilized due to the image charge attraction, and thus appears in 2PPE spectroscopy at smaller energies as the ion resonance is an intermediate state for 2PPE but a initial state of the final photoemission step. Therefore, we conclude that the unoccupied state located at 3.9 eV with respect to E_F cannot be assigned to the LUMO of TBS but rather to a higher lying unoccupied molecular state LUMO+n, in the one-electron picture.

Table 3 summarizes the energies of all electronic states observed at a TBS coverage of 1 ML. The Fermi level of the Au(111) surface serves as the reference. In addition the electronic states observed for 0.9 ML TBA on Au(111) are shown.[16]

From this the question why the LUMO level of the TBS adsorbed on Au(111) is absent in the 2PPE spectra arises. In 2PPE, the electron in the case of a charge transfer from the substrate to the adsorbate must either be directly optically excited from the substrate (resonant transition between, e.g., surface state and LUMO) or it must first be excited as a hot electron in the substrate and subsequently tunnel into the molecular resonance. Both processes are substantially impacted by the degree with which the molecular orbital mixes with the substrate states. If there is a small electronic coupling then the excitation process is unlikely. Accordingly the absence of a clear LUMO state in 2PPE suggests a weak electronic coupling for

TABLE 3: Energies of the Photoemission Spectral Features of 1 ML TBS and 0.9 ML TBA Adsorbed on Au(111),[16] Respectively[a]

	$E - E_F$ [eV]	
assignment	TBS/Au(111)	TBA/Au(111)
LUMO+n	3.9	
LUMO		1.7
n = 0 (Shockley surface state)	–0.38	–0.38
sp band	–0.87	–0.87
HOMO	–1.75	–1.85
d band	–2.0	–2.0
TBS: HOMO-1 + HOMO-2 TBA: HOMO-1	–2.65	–2.65
TBS: HOMO-3 TBA: HOMO-2 + HOMO-3	–2.9	–2.87

[a] All features are referenced to the Fermi level of Au(111).

the LUMO and the Au(111) surface. The absence of LUMO states in 2PPE has also been observed for other organic molecules on noble metals.[46−50]

Photoisomerization Ability. The electronic structure, in particular the energetic positions of the occupied states of both TBA and TBS on Au(111) are very similar (see Table 3), but contrary to TBA adsorbed on Au(111)[11,13−15] no light induced changes in the vibrational or electronic structure of surface-bound TBS are observed using different optical excitation energies ranging from 2−4.5 eV. Accordingly we propose that the photoisomerization is suppressed. In TBA/Au(111) the excitation mechanism for molecular switching has been identified to arise from a substrate-mediated charge transfer process, viz. the formation of a positive ion resonance. Thereby excitation with photon energies above ∼2.1 eV lead to the generation of hot holes in the Au d band, which rapidly relax to the top of the d band and subsequently transfer to the HOMO level of TBA induces the isomerization.[15] Even though the HOMO of TBS is located at −1.75 eV with respect to E_F, i.e., at a similar energetic position as the HOMO level of TBA on Au(111), which is −1.85 eV (see Table 3), a photoisomerization is not observed. One may speculate if the overlap between the Au d bands and the HOMO of TBS and thus the electronic coupling is weaker compared to TBA and therefore a transfer of photoexcited Au d band holes to the HOMO of TBS is unlikely. However, based on the mechanism for the photoinduced isomerization of TBA on Au(111), it is evident that a (strong) electronic coupling must be existent, i.e., some degree of hybridization between the Au d band and the HOMO of TBA, presumably via the N═N bonding or the lone pairs at the nitrogen.

In addition, it is an open question if the creation of a TBS cation would stimulate a conformational change. In order to answer this question we calculated potential energy surfaces (PES) of the neutral ground state and the cation of TBA and TBS, respectively, along the inversion angle α (the C−C−C in TBS and N−N−C angle in TBA) and the rotation angle ω. ω is the C−N═N−C dihedral angle describing a rotation around the central N═N bound for TBA. In the TBS molecule the corresponding C−C−C−C angle alone is not able to give an appropriate picture of the isomerization as reported in ref 52. Here, it was found that the H−C−C−H dihedral angle abruptly changes for relaxed scans in the C−C−C−C dihedral angle for values around 90°. Therefore we defined ω as the value of the C−C−C−C and the H−C−C−H dihedral angle as done by Noodleman and co-workers.[52] Martinez and co-workers also pointed out the importance of the pyramidalization of the C

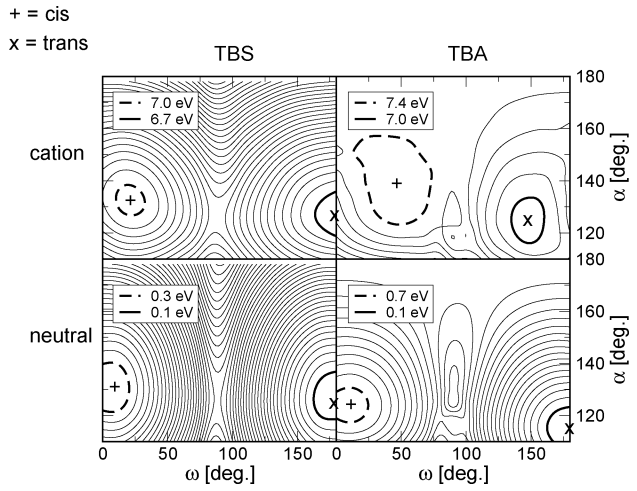

Figure 9. Shown are contour plots of PES in α and ω for the TBS molecule (left graphs) and the TBA molecule (right graphs). The lower graphs represent relaxed PES for the neutral ground state, the upper graphs the corresponding vertically ionized cationic surfaces (details see text). The contours are separated by 0.1 eV and all energies are given relative to the fully optimized trans minimum of the respective neutral molecule.

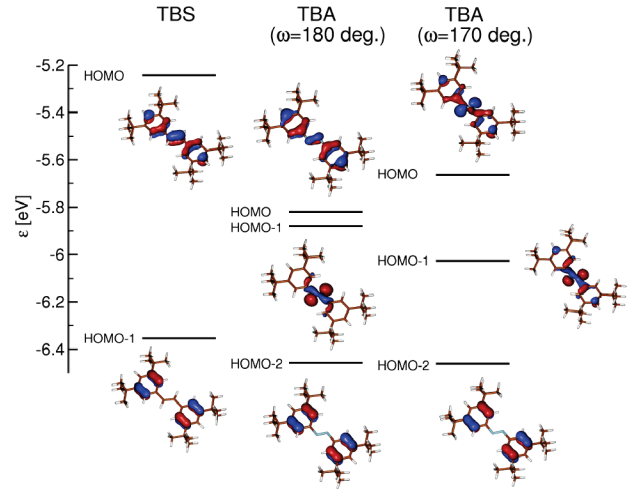

Figure 10. Shown are the energies and the shape of high lying occupied molecular orbitals for *trans*-TBS (left) and *trans*-TBA (middle). For the TBA also the orbitals for a slightly twisted relaxed configuration (ω = 170°) are displayed (right).

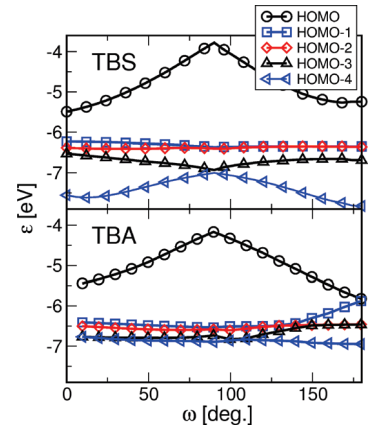

Figure 11. The energies of the high lying occupied molecular orbitals for TBS (upper graph) and for TBA (lower graph) are shown as a function of ω. The orbital energies are obtained from relaxed scan along ω for both molecules.

atoms[53] for the isomerization. However, as no such coordinate is defined for the TBA, we will focus on α and ω in the following.

The PES in α and ω for TBS and TBA are shown in Figure 9. Here, we calculated relaxed PES for the neutral ground state and the corresponding vertically ionized cationic surfaces. The PES are obtained by spline interpolation from DFT calculations with 8 points in α between 110° and 178° × 16 points in ω between 0° and 180° for the TBS molecule. For TBA we used 15 points in α between 110° and 178° × 19 points in ω between 0° and 180°. The global minimum corresponding to the *trans*-TBS is located at $\alpha_{n,TBS} = 128°$ and $\omega_{n,TBS} = 180°$ for the neutral molecule. For TBS these values are nearly unchanged after ionization, with $\alpha_{c,TBS} = 126°$ and $\omega_{c,TBS} = 180°$. The situation is different for TBA; here one gets $\alpha_{n,TBA} = 115°$ and $\omega_{n,TBA} = 180°$ compared to $\alpha_{c,TBA} = 124°$ and $\omega_{c,TBA} = 147°$. Therefore, a considerable gradient exists in α and ω after a vertical ionization.

In addition, the barriers in TBA are largely reduced after ionization. One finds $\Delta E_{n,\alpha,TBA} = 1.76$ eV and $\Delta E_{n,\omega,TBA} = 1.76$ eV compared to $\Delta E_{c,\alpha,TBA} = 0.46$ eV and $\Delta E_{c,\omega,TBA} = 0.48$ eV. Note, that the barrier of 1.76 eV for $\Delta E_{n,\omega,TBA}$ is located around $\omega = 90°$ and $\alpha = 115°$, in a region where clear traces of a conical intersection are found in the spline interpolated PES. Therefore this value is probably not really reliable. Note that according to ref.,[51] the "true" transition state for the ground state trans → cis isomerization of TBA has an activation energy of about 1.76 eV, and is located at $\omega \approx 90°$ and $\alpha \approx 180°$, indicative of simultaneous motion along ω and α. For TBS also a reduction of the barrier along ω is seen in the ionized state. In the neutral case, we get $\Delta E_{n,\omega,TBA} = 2.60$ eV, which is about 0.5 eV too high compared to estimates based on experimental data and other theoretical calculations.[52] We attribute this again to the restricted single determinant treatment, which fails in the region of the barrier. In the case of unrestricted calculations we observed large spin contaminations, i.e., the fact that the wave function becomes a mixture of singlet and triplet states, and discontinuities exactly in this region of the PES. In the cationic state we find a reduced, but still considerable barrier of 1.2 eV. In summary, at least in the gas phase trans → cis isomerization should be much more facilitated by ionization for TBA than for TBS. This is because, after an assumed vertical excitation, the TBA molecule feels larger gradients at the fixed geometry in the excited state ("Franck-Condon point") than TBS does. Also, the isomerization barrier in the cationic state is much smaller for TBA in comparison to TBS.

As already stated, we have remarkably different cationic PES for TBA and TBS. These differences can be explained by means of the Kohn−Sham orbitals for both molecules. The high lying occupied molecular orbitals for *trans*-TBS, *trans*-TBA, and a slightly twisted relaxed configuration of TBS (ω = 170°) are shown in Figure 10. Here, one can see that the HOMO is nearly identical for TBS and TBA. Furthermore, the HOMO-1 of TBS corresponds to the HOMO-2 of TBA. However, in the TBS molecule no nonbonding orbital like the HOMO-1 of TBA exists. This nonbonding orbital mixes with the π-HOMO upon rotation along ω, forming two orbitals, one slightly more bonding, i.e., energetically more stabilized than the other. Therefore, the HOMO is destabilized, while the HOMO-1 is stabilized. This trend prevails also for a further rotation along ω, as displayed in Figure 11. One can see the energies of the high lying occupied molecular orbitals for TBS and for TBA obtained from a relaxed scan along ω for both molecules. In TBS the main effect of the rotation in ω starting from the trans

isomer ($\omega = 180°$) is the destabilization of the π-HOMO. This is not surprising, as this HOMO actually forms the double bond, which hinders the rotation in ω. In the TBA molecule the HOMO is also destabilized. However, at the same time the HOMO-1 gets energetically stabilized. Therefore, in the cation after vertical ionization a gradient exists and the barrier along ω is reduced.

Conclusions

In summary, HREEL and 2PPE spectroscopy have been utilized to determine the adsorption geometry and electronic structure of the molecular switch tetra-*tert*-butyl-stilbene (TBS) adsorbed on Au(111). In addition the optically induced trans/cis isomerization ability of the surface-bound molecules is investigated. The results are compared with the tetra-*tert*-butyl-azobenzene (TBA) on Au(111), a molecule for which a photoinduced and thermally activated trans/cis isomerization is observed via reversible changes in the electronic and vibrational structure. Angular-dependent HREELS measurements show that TBS on Au(111) adsorbs in a planar configuration analogous to TBA. Several TBS-derived electronic states are observed in 2PPE. Their energetic positions have been determined and we found that the occupied molecular states, i.e., the high lying occupied molecular orbitals, possess similar energetic positions as obtained for TBA/Au(111). In contrast to TBA/Au(111) no photoinduced changes in the geometry or electronic structure of TBS are observed. Therefore we conclude that the photoisomerization is suppressed. Whereas the molecular switching in TBA is driven by the generation of a positive ion resonance (cation) via a charge transfer of holes from the Au d band to the HOMO level of TBA, this mechanism is obversely not efficient in TBS/Au(111) even though the HOMO of TBS is at a similar energetic position. Quantum chemical calculations of the potential energy surfaces for the free TBA and TBS molecule corroborate this conclusion. They indicate that for the TBA cation larger gradients at the Franck−Condon point than for the TBS cation exist. Furthermore in the cationic states the barrier is strongly reduced in TBA compared to TBS.

Further experiments, including the determination of the geometry, electronic structure and the photoisomerization ability of the imine (−N═CH−) analogue adsorbed on Au(111) in order to gain a comparative insight into the switching properties, are in progress. This may allow us to get a general picture of the photoinduced trans/cis isomerization properties of surface-bound molecular switches.

Acknowledgment. This work has been supported by the Deutsche Forschungsgemeinschaft through the SFB 658 "Elementary processes in molecular switches at surfaces" (Projects B1, B8, and C2).

Supporting Information Available: Synthesis of *trans*-3,3′,5,5′-tetra-*tert*-butyl-stilbene and its isomerization behavior in solution. This material is available free of charge via the Internet at http://pubs.acs.org.

References and Notes

(1) Waldeck, D. H. *Chem. Rev.* **1991**, *91*, 415.
(2) Maier, H. *Angew. Chem., Int. Ed.* **1992**, *31*, 1399.
(3) Saltiel, J.; Sun, Y.-P. In *Photochromism -Molecules and Systems*; Dürr, H., Bouas-Laurent, H., Eds.; Elsevier: Amsterdam, 2003.
(4) Feringa, B. L. *Molecular Switches*; Wiley-VCH: Weinheim, Germany, 2001.
(5) Fanghänel, D. ; Timpe, G.; Orthman, V. in *Organic Photochromes*; El'tsov, A. V., Ed.; Consultants Bureau: New York, 1990.
(6) Tamai, N.; Miyasaka, O. H. *Chem. Rev.* **2000**, *100*, 1875.
(7) Rau, H. In *Photochromism - Molecules and Systems*; Dürr, H., Bouas-Laurent, H., Eds.; Elsevier: Amsterdam, 2003.
(8) Balzani, V., Credi, A., Venturi, M., Eds.; *Molecular devices and machines - A journey into the nanoworld*; Wiley-VCH: Weinheim, Germany, 2003.
(9) Browne, W. R.; Feringa, B. L. *Nat. Nanotechnol.* **2006**, *1*, 25.
(10) Balzani, V.; Credi, A.; Venturi, M. *ChemPhysChem* **2008**, *9*, 202.
(11) Hagen, S.; Leyssner, F.; Nandi, D.; Wolf, M.; Tegeder, P. *Chem. Phys. Lett.* **2007**, *444*, 85.
(12) Comstock, M. J.; Levy, N.; Kirakosian, A.; Cho, J.; Lauterwasser, F.; Harvey, J. H.; Strubbe, D. A.; Fréchet, J. M. J.; Trauner, D.; Louie, S. G.; Crommie, M. F. *Phys. Rev. Lett.* **2007**, *99*, 038301/1.
(13) Óvári, L.; Wolf, M.; Tegeder, P. *J. Phys. Chem. C* **2007**, *111*, 15370.
(14) Hagen, S.; Kate, P.; Peters, M. V.; Hecht, S.; Wolf, M.; Tegeder, P. *Appl. Phys. A: Mater. Sci. Process.* **2008**, *93*, 253.
(15) Hagen, S.; Kate, P.; Leyssner, F.; Nandi, D.; Wolf, M.; Tegeder, P. *J. Chem. Phys.* **2008**, *129*, 164102.
(16) Wolf, M.; Tegeder, P. *Surf. Sci.* **2009**, *603*, 1506.
(17) Tegeder, P.; Hagen, S.; Leyssner, F.; Peters, M. V.; Hecht, S.; Klamroth, T.; Saalfrank, P.; Wolf, M. *Appl. Phys. A: Mater. Sci. Process.* **2007**, *88*, 465.
(18) Cortés, R.; Mascaraque, A.; Schmidt-Weber, P.; Dil, H.; Kampen, T. U.; Horn, K. *Nano Lett.* **2008**, *8*, 4162.
(19) Schmidt, P. M.; Horn, K.; Dil, J. H.; Kampen, T. U. *Surf. Sci.* **2007**, *601*, 1775.
(20) Tsai, C.-S.; Su, C.; Wang, J.-K.; Lin, C.-J. *Langmuir* **2003**, *19*, 822.
(21) Chou, L.-W.; Lee, Y.-R.; Wei, C.-M.; Jiang, J.-C.; Lin, J.-C.; Wang, J.-K. *J. Phys. Chem. C* **2009**, *113*, 208.
(22) Tsai, C.-S.; Wang, J.-K.; Skodje, R. T.; Lin, J.-C. *J. Am. Chem. Soc.* **2005**, *127*, 10788.
(23) Slayton, R. M.; Franklin, N. R.; Tro, N. J. *J. Phys. Chem.* **1996**, *100*, 15554.
(24) Ibach, H.; Mills, D. *Electron energy loss spectroscopy and surface vibrations*; Academic Press: New York, 1982.
(25) Hoffmann, F. M. *Surf. Sci. Rep.* **1983**, *3*, 107.
(26) Frisch, M. J. Trucks, G. W. Schlegel, H. B. Scuseria, G. E. Robb, M. A. Cheeseman, J. R. Montgomery, J. A., Jr. ; Vreven, T. Kudin, K. N. Burant, J. C. Millam, J. M. Iyengar, S. S. Tomasi, J. Barone, V. Mennucci, B. Cossi, M. Scalmani, G. Rega, N. Petersson, G. A. Nakatsuji, H. Hada, M. Ehara, M. Toyota, K. Fukuda, R. Hasegawa, J. Ishida, M. Nakajima, T. Honda, Y. Kitao, O. Nakai, H. Klene, M. Li, X. Knox, J. E. Hratchian, H. P. Cross, J. B. Adamo, C. Jaramillo, J. Gomperts, R. Stratmann, R. E. Yazyev, O. Austin, A. J. Cammi, R. Pomelli, C. Ochterski, J. W. Ayala, P. Y. Morokuma, K. Voth, G. A. Salvador, P. Dannenberg, J. J. Zakrzewski, V. G. Dapprich, S. Daniels, A. D. Strain, M. C. Farkas, O. Malick, D. K. Rabuck, A. D. Raghavachari, K. Foresman, J. B. Ortiz, J. V. Cui, Q. Baboul, A. G. Clifford, S. Cioslowski, J. Stefanov, B. B. Liu, G. Liashenko, A. Piskorz, P. Komaromi, I. Martin, R. L. Fox, D. J. Keith, T. Al-Laham, M. A. Peng, C. Y. Nanayakkara, A. Challacombe, M. Gill, P. M. W. Johnson, B. Chen, W. Wong, M. W. Gonzalez, C., Pople, J. A. *Gaussian 03*, revision C.02; Gaussian, Inc.: Wallingford CT, 2004.
(27) Becke, A. D. *J. Chem. Phys.* **1993**, *98*, 5648.
(28) Hariharan, P. C.; Pople, J. A. *Theoret. Chim. Acta* **1973**, *28*, 213.
(29) Ditchfield, R.; Hehre, W. J.; Pople, J. A. *J. Chem. Phys.* **1971**, *54*, 724.
(30) Hehre, W. J.; Ditchfield, R.; Pople, J. A. *J. Chem. Phys.* **1972**, *56*, 2257.
(31) Óvári, L.; Schwarz, J.; Peters, M. V.; Hecht, S.; Wolf, M.; Tegeder, P. *Int. J. Mass. Spectrom.* **2008**, *277*, 223.
(32) Xi, M.; Wang, M. X.; Jo, S. K.; Bent, B. E.; Stevens, P. *J. Chem. Phys.* **1995**, *101*, 9122.
(33) Rockey, T. J.; Yang, M.; Dai, H. L. *J. Phys. Chem. B* **2006**, *110*, 19973.
(34) Vondrak, T.; Zhu, X.-Y. *J. Phys. Chem. B* **1999**, *103*, 3449.
(35) Zhong, Q.; Gahl, C.; Wolf, M. *Surf. Sci.* **2002**, *496*, 21.
(36) Meić, Z.; Güsten, H. *Spectrochem. Acta A* **1978**, *34*, 101.
(37) Arenas, J. F.; López, I.; Otero, J. C.; Marcos, J. I. *J. Phys. Chem.* **1995**, *99*, 11392.
(38) Choi, C. H.; Kertesz, M. *J. Phys. Chem. A* **1997**, *101*, 3823.
(39) Peters, M. V. Ph.D. Thesis, Humboldt Universität Berlin, 2008.
(40) Alemani, M.; Selvanathan, S.; Ample, F.; Peters, M. V.; Rieder, K.-H.; Moresco, F.; Joachim, Ch.; Hecht, H.; Grill, L. *J. Phys. Chem. C* **2008**, *112*, 10509.
(41) Alemani, M.; Peters, M. V.; Hecht, S.; Rieder, K.-H.; Moresco, F.; Grill, L. *J. Am. Chem. Soc.* **2006**, *128*, 14446.
(42) Reinert, F.; Nicolay, G.; Schmidt, S.; Ehm, D.; Hüfner, S. *Phys. Rev. B* **2001**, *63*, 115415.
(43) Eckhart, H.; Fritsche, L.; Noffke, J. *J. Phys. F: Met. Phys.* **1984**, *14*, 97.
(44) Courths, R.; Zimmer, H.-G.; Goldmann, A.; Saalfeld, H. *Phys. Rev. B* **1986**, *34*, 3577.

(45) Fauster, T.; Steinmann, W. In *Electromagnetic Waves: Recent Developments in Research*; Halevi, P., Ed.; Elsevier: Amsterdam, 1995.
(46) Lindstrom, C. D.; Muntwiler, M.; Zhu, X.-Y. *J. Chem. Phys. B* **2007**, *111*, 6913.
(47) Gaffney, K. J.; Wong, C. M.; Liu, S. H.; Miller, A. D.; McNeill, J. D.; Harris, C. B. *Chem. Phys.* **2000**, *251*, 99.
(48) Velic, D.; Hotzel, A.; Wolf, M.; Ertl, G.*J. Chem. Phys.* **1989**, *109*, 9155.
(49) Gaffney, K. J.; Miller, A. D.; Liu, S. H.; Harris, C. B. *J. Phys. Chem. B* **2001**, *105*, 9031.
(50) Wang, H.; Dutton, G.; Zhu, X.-Y. *J. Phys. Chem. B* **2000**, *104*, 10332.
(51) Dokić, J.; Gothe, M.; Wirth, J.; Peters, M. V.; Schwarz, J.; Hecht, S.; Saalfrank, P. *J. Phys. Chem. A* **2009**, *113*, 6763.
(52) Han, W.-G.; Lovell, T.; Liu, T.; Noodleman, L. *ChemPhysChem* **2002**, *3*, 167.
(53) Quenneville, J.; Martinez, T. J. *J. Phys. Chem. A* **2003**, *107*, 829.

JP909684X